RSC Advances

ROYAL SOCIETY OF CHEMISTRY

www.rsc.org/advances

Pd Nanoparticles Supported On Reduced Graphene-*E. coli* Hybrid With Enhanced Crystallinity In Bacterial Biomass

Rachel E. Priestley[†], Alexander Mansfield[†], Joshua Bye[†], Kevin Deplanche[‡], Ana B. Jorge[§], Dan Brett, Lynne E. Macaskie[‡§], Surbhi Sharma*[†]

[†]Centre for Hydrogen and Fuel Cell Research, School of Chemical Engineering, University of Birmingham, Edgbaston, Birmingham, B15 2TT, UK

[‡]Unit of Functional Bionanomaterials, School of Bioscience, University of Birmingham, Edgbaston, Birmingham, B15 2TT, UK

[§]UCL Chemical Engineering Department, Electrochemical Innovation Lab, Torrington Place, WC1E 7JE, London, UK

* Address correspondence to: s.sharma.1@bham.ac.uk

ABSTRACT

A novel method for simultaneous reduction of graphene oxide (GO) and palladium salt, Pd (II), using *Escherichia coli* in the separate presence of two different mild reducing agents (hydrogen and formate) is investigated to successfully produce reduced GO (rGO)-biomass/Pd hybrid material for potential use as an electrocatalyst. Transmission electron microscopy, X-ray diffraction, thermo-gravimetric analysis, X-ray photoelectron spectroscopy and Raman microscopy demonstrate the successful reduction of Pd (II), GO and the biomass, resulting in the formation of Pd nanoparticles (PdNPs) on an rGO-biomass hybrid. The distribution of the NPs was found to be dependent on the type of reducing agent. PdNPs formed on rGO sheets showed relatively uniform distribution and size control (2-5 nm), whereas PdNPs on the bacterial scaffold were larger (up to 10 nm in size). Raman spectroscopy studies suggest that the presence of Pd leads to oxygen reduction and increased crystallinity in the bacterial biomass. Previous studies have suggested the potential for a bacterially-supported Pd electrocatalyst in fuel cells and, independently, the suitability of rGO as a support for PdNPs. This study confirms the simultaneous bacterial reduction of Pd (II) and GO and the association between the bacterial cells and rGO. We suggest that the simultaneous presence of *E. coli* and mild reducing agent together with GO and Pd (II) creates an interactive and synergistic environment in a hybrid material to allow a) better control of PdNP size and distribution both on the inside of the bacterial membrane and on the rGO sheets and b) increased crystallinity of the bacterial biomass compared to systems with bacteria alone.

Keywords: E.coli; reduced graphene; BioPd; Palladium nanoparticles; catalyst-support;

INTRODUCTION

Palladium (Pd) is a ubiquitous catalyst used in automotive[1], oil refining[2], polyester manufacturing[3] and as a synthesis platform for fine chemicals. It is also a promising candidate for use as an electrocatalyst, to reduce the dependence on platinum (Pt) for applications such as water electrolysis and polymer electrolyte membrane fuel cell (PEMFC) catalysts, since it has many properties similar to Pt including its electronic and face centred cubic crystal structure. While both Pt and Pd are susceptible to durability issues and carbon monoxide poisoning, the high price and limited availability of Pt necessitate the search for alternatives. Recent studies show that palladium nanoparticles (PdNPs) can be used as an oxygen reduction catalyst in a PEMFC cathode with 80% of the current density and 87% of the peak power density when compared with commercial Pt/C[4]. Pd is significantly cheaper than Pt and more than 50 times more abundant[5]. Furthermore, recent studies on Pd have revealed that it has greater resistance to carbon monoxide poisoning when used as a PEMFC catalyst compared with Pt[6,7]. Limited supply of precious metals (like Pt and Pd) has led to studies on waste metal recovery for maximising the utilisation of these precious metals.

Murray et al.[8] used microbial reduction of soluble palladium (II) salt to recover Pd and Pt from spent automotive catalyst leachates in the form of nanoparticles on the surface of bacterial cells and these metals, biorecovered from a waste, were able to function as the anode catalyst in a PEMFC after processing.[45] Bioreduction, first reported by Lloyd et al.[9] using *Desulfovibrio desulfuricans*, and on the surface of various other bacteria, such as *Shewanella oneidensis* and *Escherichia coli* [10-12] has generated substantial interest in this field. Yong et al.[13] showed that by increasing the biomass:Pd ratio, smaller nanoparticles could be produced, while a report by Sobjerg et al.[14] demonstrated further size and shape control. Yong et al.[14] found that Pd produced in this way (BioPd) gives an effective anode catalyst in PEMFCs after sintering. The low conductivity of the interstitial biomass[12] needs to be addressed in order to improve the performance and efficiency of such ~~a~~ catalyst-support systems. The properties of the catalyst support used also play an important role in determining the particle size uniformity, particle distribution, catalyst efficiency and lifetime[15]. 'Carbonised' BioPd formed by sintering the biomass-Pd(0) composite was used in a fuel cell application,[14] while electron

paramagnetic resonance (EPR) measurements suggested that, when mixed with commercial activated carbon, there is evidence of electron transport between the BioPd and the activated carbon[16]. Use of sintered BioPd in a PEMFC is reported to display a power density close to that measured using a commercial Pd/C catalyst. However, other residual elements remaining in the support material may be detrimental to the electrocatalytic activity; hence there is a need to explore other conductive supports where changes to the biomass component can be minimised. It is, therefore, essential to explore techniques to reduce Pd loading, control nanoparticle size, and also retain conductivity via proximity of PdNPs to the conductive material to facilitate electron transport between Pd and the electrode.

Recent studies have shown that some of the bacteria that exhibit metal-reducing capabilities can also reduce graphene oxide (GO), producing reduced graphene oxide (rGO) with physical and electrochemical properties comparable to chemically reduced GO[17-21]. Several studies have investigated the reduction of GO through various chemical routes to produce reduced graphene for application as catalyst support for metal nanoparticles in various catalytic applications (due to the outstanding electronic and surface properties of graphene)~~,~~, including polymer electrolyte fuel cells .[22-31] However, these methods generally use high concentrations of Pt/metal precursors. The use of bacteria for GO reduction has attracted attention only recently. Yuan et al.[32] have shown that, in a microbial fuel cell, GO is reduced *in-situ* to form a biomass-graphene network that improves conductivity and hence power output of the cell. Compared to the various chemical/ non-biological methods, biological reduction methods could allow better conservation of metal by the nanoscale scaffolding contributed by the bacterial surface, as well as stability against agglomeration.[33] While many previous studies have suggested the potential for a bacterially-supported Pd electrocatalyst in fuel cells and, independently, the suitability of rGO as a support for PdNPs, no studies so far have investigated the simultaneous bacterial reduction of Pd (II) salt and GO and the resultant structure and potential interactions between these reactive species.

In this study, we report the production of a Pd/rGO composite using H_2 or sodium formate by the simultaneous bacterial reduction of GO and Pd (II) salt supported by *E. coli*. The processing of the Pd, GO and *E. coli* together with a reducing agent means that the product exhibits enhanced reduction and

altered structure. This work reveals that the presence of Pd nanoparticles and/or the nucleation process may have a catalytic effect in structuring the carbon present in the biomass, which could significantly enhance the Pd-biomass interaction and enable a more conductive response of the electrocatalyst overall.

METHODS AND MATERIALS

Reduction of GO/Pd

The graphene oxide was prepared using a modified Hummers' method. Sodium tetrachloropalladate (Na_2PdCl_4) was used as the Pd precursor and the bacterial strain used in this study was *E. coli* MC4100. The bacterial culture[11] (stored anaerobically under oxygen-free nitrogen (OFN) at 4°C in a rubber-sealed bottle and used within 48 hours of culturing) was used to separately inoculate three solutions, namely; (i) oxygen-free Pd (II) salt solution at a loading of 25 wt.% Pd, (ii) GO solution at a loading of 15 wt%, and (iii) a mixture of the Pd (II) salt and GO solution, along with appropriate control samples (Tables 1, S1). All samples were inoculated and stored in sealed bottles. The inoculated solutions and controls were incubated at 30 °C for ~1 h to allow biosorption of Pd (II) on to the cell surfaces and then a reducing agent (electron donor) was added as described. Half of each mixture was reduced using 500 mM degassed sodium formate stock solution (final concentration 20 mM) and then the solution was transferred to a heater/shaker at 37 °C for at least 24 hours. The other half was reduced using hydrogen gas, which was bubbled through the mixture for 15 minutes, and an excess of hydrogen was added into the headspace of the sealed bottles (via a syringe through the rubber stopper). After the reduction, samples were harvested by centrifugation and the supernatant was tested for the presence of residual palladium using the tin chloride assay as described elsewhere[11]. For simplicity, all samples were given acronyms of the format 'sample(electron donor)' and all samples prepared with *E. coli* have a prefix 'B' representing 'Bio-synthesis'. So a sample of Pd and GO reduced in the presence of *E. coli* using H_2 as the e^- donor is denoted as B-rGO/Pd(H) The samples produced and the respective acronyms used throughout the rest of this paper are listed in

Table 1. In order to ascertain the effect of each of the electron donors and the presence of *E. coli* on the reduction process, various control samples were also produced using only bacteria, hydrogen or formate as reducing agent/e^- donor and were given acronyms using the same convention as above. A list of all control samples (Table S1) and further details of the preparation of a bacterial culture of *E. coli* MC4100, GO and Pd (II) salt solution can be found in the supporting information.

Control /Test samples	Acronym
E. coli, GO, H_2	B-rGO(H)
E. coli, GO, Formate	B-rGO(F)
E. coli, Pd, H_2	B-Pd(H)
E. coli, Pd, Formate	B-Pd(F)
E. coli, GO, Pd, H_2	B-rGO/Pd(H)
E. coli, GO, Pd, Formate	B-rGO/Pd(F)

Table 1: Sample constituents and acronyms for test samples and main control samples used in the study.

The as prepared Pd, *E.coli*, rGO hybrid samples, were not washed in acetone which is known to improve the accessibility of intracellular Pd NPs. This is a standard way of breaking down the permeability barrier by disrupting the cell membranes[46, 47]. This was not used in the present study as we wished to visualise the interactions of the GO/rGO with the bacterial surfaces.

Characterisation of Materials

TEM examination of cell sections used a JEOL 1200X electron microscope and for whole cells used a JEOL 2100 electron microscope with an Oxford instruments X-Max 80T detector for energy dispersive x-ray microanalysis (EDX). Powder XRD analysis was carried out on a Bruker D2 Phaser diffractometer with a monochromatic Co Kα radiation (wavelength = 1.79026 Å). FT-IR analysis was carried out on a Varian 660 IR FTIR Spectrometer with Pike MIRacle diamond ATR. TGA

experiments were conducted using samples between 9 mg and 11 mg on a Netzsch TG 209 F1 Libra over the temperature range 25 - 800°C. The heating rate was 5 °C/min and a gas stream of 50:50 N_2 and O_2 at a combined flow rate of 50 mL/min was used in an environment of N_2 and O_2. XPS analysis was conducted on an Al K-Alpha (Thermo Scientific) instrument. Data was collected from the surface of thin film samples and analysis was performed using Casa XPS. Calibration was carried out by alignment of the spectra with reference to the C 1s line at 284.5 eV associated with graphitic carbon, and a Shirley background correction was applied. Raman spectroscopy was conducted on a Renishaw InVia Reflex Confocal Raman microscope using a 514 nm laser. Details of the preparation of samples for various characterisations are included in the supporting information.

RESULTS AND DISCUSSION

Transmission electron microscopy was used to image the simultaneously reduced GO and Pd (II) samples. The samples were prepared and imaged in two different ways to enhance our understanding of PdNPs distribution and interaction between GO/rGO sheets and *E. coli* cells. At first, images (Figure 1a, b, d and e) were obtained using microtome-sectioned cells (prepared using standard fixation, embedding and resin sectioning protocols). Although these provided information of PdNPs distribution inside the cells, high resolution imaging was restricted due to extensive charging caused by the non-conductive resins. Hence, another set of samples was prepared by dropping a small amount of dilute sample solution onto a copper grid, which is a commonly used sample preparation method for metal nanoparticles on carbon supports. The images thus obtained (Figure 1c and 1f) provided high resolution images of metal nanoparticles and rGO sheets, allowing visualisation of particle sizes on rGO as well as *E. coli*. The TEM images and energy dispersive x-ray (EDX) analysis (Figure S2) confirmed the presence of Pd nanoparticles (PdNPs) within (Figure 1a-e) and on the surface of the *E. coli* cells as well as on rGO sheets. However, no Pd nanoparticles were observed outside or independently of the intact cells and rGO sheets. The GO/rGO sheets appeared to be between 20-100 nm and the PdNPs appear to nucleate on the cells or the GO sheets and are not visible independent of a support. Figure 1a and 1e, showing TEM images for B-rGO/Pd(F) and B-rGO/Pd(H) respectively,

show that the rGO sheets are interspersed between the cells and that they tend to have higher distribution near the cell suggesting possible electron transfer-like interactions between GO and *E. coli* (similar to the Mtr respiratory pathway in *Shewanella oneidensis*, as suggested by Jiao et al.[34]) eventually leading to GO reduction. While GO sheets appear to have a tendency to wrap around the bacterial cells, contrary to other literature[19], the GO/rGO sheet edges did not appear to pierce through the cells.

Figure 1a-c show images of B-rGO/Pd(F) samples while images Figure 1d-f show images of B-rGO/Pd(H) samples. Comparison of images b and c with d and e in Figure 1 clearly revealed that when formate was used as the e^- donor/ reducing agent, the PdNPs are more uniformly sized and distributed (Figure 1b), whereas when H_2 was used (Figure 1d and e) more PdNPs were formed on the cell surface (i.e close to the outer membrane) and as a result the particles are more likely to agglomerate (Figure 1e), leading to larger particle size. XRD analysis (discussed further below) also confirmed larger particle sizes for both test and control samples prepared using H_2 as the e^- donor. In sectioned images, some larger PdNPs are visible on edges of long micron sized sheet like structures (circled in red in Figure 1d). These sheet-like structures are possibly ruptured cell membranes as they are too long to be rGO sheets. It has been observed elsewhere that cells that have been disabled either by genetic removal of key enzymes[11] or stressed by toxic chemicals[45] can respond by making large nanoparticles outside the cell, presumably via leakage of contents from damaged cells and uncontrolled, 'runaway' NP formation on released additional nucleation sites. Flow cytometry studies are planned to look at the 'robustness' of the bacteria under the dual stress of palladisation and potential graphene penetration in the next phase of the work.

Imaging of samples produced by drop-drying the solution onto a copper grid (Figures 1c and 1f and S1b) showed the surface of rGO sheets decorated with very small (2-5 nm) Pd nanoparticles in both H_2 and formate conditions. Formate has been used as a mild reducing agent for reduction of Pd (II) to PdNPs[35] and in the presence of GO, PdNPs are likely to nucleate on the oxygen defects in a reducing environment (similar to Pt nanoparticles[28]). Figure 1c shows a high resolution image of the rGO sheets clustering around the cell surface (circled in 1c). The inset in Figure 1c shows a large (20-30

nm) individual nanoparticle extruded within a cell membrane vesicle, and the lattice fringes revealed a spacing of 0.223 nm, in agreement with the spacing of Pd (111) lattice planes, 0.2246 nm (JCPDS 46-1043). Interestingly, all PdNPs on rGO sheets showed smaller size and more uniform size distributions compared to the PdNPs formed inside the bacterial cells. This is speculated to be due to two reasons: a) the bacterial cells have a quicker and/or greater uptake of the Pd (II) salt, leading to more PdNPs formation and resulting in agglomeration and larger particle sizes; b) the rate of nucleation and growth of PdNPs inside the bacterial cells is faster compared to that on rGO sheets. Figure S1c also shows small (<5-10 nm) PdNPs on the rGO sheets as seen in the B-rGO/Pd(H) samples and those circled gave lattice spacing of (1): 0.243 nm, 0.239 nm, (2): 0.210 nm, (3): 0.204 nm, which is within 1.5% of the reference value. Such deviations are expected due to the varying orientations of the NPs with respect to the electron beam[36]. The Pd nanoparticle size was found to vary from 20-30 nm to 2-5 nm depending upon the location of the nanoparticles. Particles inside the *E.coli* and in the absence of GO were found to be bigger while those formed on the rGO sheets showed a size distribution of 2-5 nm. Most traditional methods used for preparation of catalyst nanoparticles are reported to form nanoparticles in the range of 2-5 nm or at least below 10 nm. The nanoparticles we prepared in this current method show relatively larger size variation. However, it is evident from the TEM images that there is more agglomeration of Pd nanoparticles inside the bacterial cell when H2 is used and also when no GO is present. Thus, agglomeration and particle size is dependent on, (a) the Pd(II) uptake of the cell and also on, (b) the type of e donor available. Further studies will be undertaken to optimise the nanoparticles size using these parameters for electrochemical studies during the next phase.

Figure 1f (circled) shows the edges of a stack of 8 rGO sheets with PdNPs attached to both basal and edge planes. The sheet separation was found to be 0.338 nm, which is in agreement with the separation of graphene sheets (0.34 nm). EDX analysis (Figure S2) carried out at different positions on the samples confirmed the presence of carbon, palladium and oxygen in the cell and rGO areas. The presence of small amounts of P, Na and S was also found in the bacterial cells, as expected for biological material.

The XRD pattern for GO (Figure 2a) consists of the typical graphitic carbon (002) peak around 2θ = 30.6° corresponding to a *d*-spacing of 0.34 nm, as well as another broad C (002) peak shifted down to around 2θ = 13.5 - 15.3°, indicating that a major proportion of the carbon sheets have been separated by a larger distance (0.67 - 0.76 nm) by the oxygen functional groups added by the oxidation process[22]. As GO is reduced, the peak at 2θ = 30.6° should increase in intensity, and the lower 2θ peak is reduced. In comparison, the scan for B-rGO(H) (Figure 2a) revealed two relatively sharp peaks for carbon. The first is shifted to a lower 2θ angle (~10°) and is less intense than in GO, while the 30.6° peak displayed an increase in intensity, indicating only a partial reduction of GO. However, the scan for B-rGO(F) showed almost a complete loss of the peak at low 2θ values, while the 30.6° peak showed a clear increase in the intensity, suggesting that the reduction with formate was more effective compared to that with hydrogen. Interestingly, in the presence of Pd (Figure 2b) both B-rGO/Pd(H) and B-rGO/Pd(F), did not reveal any peak at lower 2θ values, suggesting that most or all of the oxygen functional groups on the GO sheets were removed. This is most likely due to the fact that the reduction of GO and nucleation of NPs on the GO surface are simultaneous processes. As metal NP nucleation takes place at the oxygen defect sites, more oxygen groups are reduced[28]. The XRD analysis (Figure 2b) for B-rGO/Pd(H) and B-rGO/Pd(F) samples further revealed the characteristic peaks for Pd(111) and Pd (002) (peak positions reveal plane spacing of 0.2246 nm and 0.1945 nm respectively confirmed by JCPDS, card no. 05-0681) for both B-rGO/Pd(H) and B-rGO/Pd(F). The powder patterns also confirmed the TEM observations of particle sizes. Calculations using the Scherrer equation indicated that PdNPs which nucleated and grew in the presence of GO using *E. coli* and H_2 (i.e. B-rGO/Pd(H) were on average 10-15 nm, while the PdNPs which nucleated in the presence of GO using *E. coli* and formate (i.e. B-rGO/Pd(F)) were 5-10 nm. These Pd peaks were found to be broad, compared to sharp peaks (Figure S3) for control samples Pd(H) and Pd(F) (particle size of 20-25 nm) where Pd was reduced in the absence of *E. coli,* demonstrating that the use of *E. coli* promotes formation of smaller nanoparticles. No Pd peaks were found in the XRD patterns for control samples B-Pd and B-rGO/Pd (Figure S3) i.e. in the absence of any electron donor, suggesting that Pd (II) salt is not reduced in the absence of a reducing agent. However, the formation of amorphous small Pd-NPs or single atoms of Pd(0) cannot be precluded.

Similarly, no shift or change was observed in the 2θ~10° peak for control sample B-rGO (Figure S3a) confirming that bacteria alone cannot promote GO reduction. On the other hand, control samples rGO(H) and rGO(F) showed the lower 2θ peak shifted slightly (2θ~14°) and was significantly sharper and more intense compared to that of starting GO; in addition, a small, very broad graphitic carbon peak near 2θ~30° indicated some reduction of GO in the presence of mild electron donors (Figure S3a).

No Pd peaks were found in the XRD patterns for control samples B-Pd and B-rGO/Pd in Figure S3 (i.e. in the absence of any electron donor), confirming that Pd (II) salt is not reduced in the absence of a reducing agent. This, however, does not exclude the possibility of very small Pd-NPs (e.g. 2 nm or smaller which are invisible to XRD and appear as amorphous). Nevertheless, using XPS in this study no evidence was seen for 'endogenous' reduction of Pd(II), i.e. in the absence of added electron donor. Given time, Pd(II) reduces chemically under H_2 (and with formate) and, indeed, killed cells or formate alone show very slow Pd(II) reduction[11]. The presence of live bacteria (being enzymatic and hence catalytic) not only accelerates what would happen anyway, but also 'steers' to some extent the location(s) of the nucleation and nanoparticle growth[48]. Hence, the *E. coli* provides a suitable 'environment' for the Pd salt and the e^- donor to be adsorbed so that the reduction reaction can take place, as well as acceleration of this reduction.

Control samples rGO/Pd(H) and rGO/Pd(F), i.e. without *E. coli* (Figure S3c), revealed sharp Pd peaks indicating reduction of Pd (II) but forming significantly larger crystals and little or no reduction of GO. Moreover, XRD data as shown in figure S3, S5(a) and S5 (b) confirmed that no reduction of GO occurs in the presence of e-donor (H_2 or formate) alone. On the other hand significant GO reduction was observed when *E. coli* was present along with the reducing agent (figure 2a and figure 3), confirming that GO reduction occurs in the presence of *E. coli* due to possible synergistic interactions. This further suggests that there is electron exchange between bacterial hydrogenases and GO promoting GO reduction and possibly allowing size control of PdNPs on rGO sheets. Thus, the XRD patterns from various samples and control samples confirmed that the presence of the bacterial cells as well as a mild reducing agent (either H_2 or formate), have a vital role to play not only in the reduction

of both GO and Pd (II) but also in controlling the PdNP size and distribution. Moreover, the presence of Pd further enhances the reduction of GO.

Thermogravimetric analysis was used to provide information about the thermal stability and composition of the samples. The results for GO (Figure 2c) show the typical three stages of the breakdown of GO in the presence of oxygen[37]. However, all samples with rGO or no GO content revealed significantly less weight loss below 200 °C, indicating lower water content compared to GO. In the *E. coli* alone, and in all samples containing *E. coli* (with or without rGO), the removal of oxygen functional groups occurred at around 300 °C, suggesting that most of these are from the bacteria and that GO has been reduced during the reduction process. The removal of the carbon skeleton occurred around 500 °C for *E. coli* alone, while for the samples not containing Pd (Figure 2c) it occurred between 500-600 °C. The breakdown of the carbon in B-rGO(H) and B-rGO(F) occurred over a wider temperature range and therefore appears to be a combination of the breakdown of the carbon content in bacteria and GO. Samples containing Pd (Figure 2d) showed a lower final breakdown temperature, which was just below 400 °C. This could be due to Pd catalysing the breakdown of carbon. It is, therefore, suggested that the presence of the Pd is altering the structure of the carbon and thus its thermal behaviour. This argument is supported by evidence from XPS and Raman spectroscopy discussed in later sections. Studies using Pt have reported a higher temperature for carbon breakdown[18] while Pd is reported to catalyse the formation of C-C bonds[31]. However, samples with GO show a further 2-3 wt.% loss between 600-800 °C which is similar to other TGA studies[28] reported on metal nanoparticle/rGO samples, showing the structural stability of GO. There was some residue in all samples, which was due to residual elements from the production processes (chemicals used in production of GO, bacterial suspension medium, etc.) as well as substances found in the bacterial cells (phosphorus, sulphur and trace metallic residues from proteins etc). The residue in samples containing Pd is largely the metal constituent, and 30-40 wt.%, which is higher than the original loading of 25 wt.%. This can be attributed to the mass loss in GO and bacteria during the reduction processes leading to higher metallic content in the product. Control samples without GO, (B-Pd(H) and B-Pd(F)) showed a higher Pd residue, suggesting higher intake of Pd (II) salt resulting

in more Pd nucleation and growth (i.e. in the absence of GO 'competing' for available Pd (II)). Among these, the use of formate seems to enhance the Pd nucleation further than H_2. The lower Pd wt.% in B-rGO/Pd(F) and B-rGO/Pd(H) samples supports the theory that there is a possible competing process(es) between GO and *E. coli* for the uptake of Pd (II). As observed in TEM images, the nucleation and growth process on GO/rGO sheets appears to be slower compared to *E. coli*, leading to smaller and well distributed particles on rGO. Consequently, in the presence of GO, *E. coli* is not able to take up as much Pd (II) which it is otherwise capable of, resulting in a lower final Pd loading in the bacterial content of the overall sample.

Sample / Element	Average percentage area of elemental regions							
	GO	*E. coli*	B-rGO(H)	B-rGO(F)	B-Pd(H)	B-Pd(F)	B-rGO/Pd(H)	B-rGO/Pd(F)
C 1s	76.3	67.2	72.4	71.4	75.4	75.2	75.1	73.4
N 1s	-	9.1	6.9	9.0	5.7	5.8	8.4	7.5
O 1s	23.7	22.2	19.3	18.6	18.2	18.0	15.9	18.2
P 2p	-	1.4	1.5	1.1	-	-	-	-
Pd 3d	-	-	-	-	0.7	1.0	0.5	0.9

Table 2: Average percentages of elements in surface layers of various samples as obtained using XPS data

XPS analysis was carried out in order to further and more accurately probe the proportions of different elements and types of bonds in the rGO sheets and bacterial surface layers. High resolution spectra of carbon, oxygen and palladium regions were deconvoluted using binding energies found in the literature. Components of spectra were allowed a full width at half maximum (FWHM) of

approximately 1 eV and given a Gaussian-Lorentzian line shape (GL(30)). Table 2 gives the elemental composition of the samples as calculated from the survey scans. Since XPS is a surface analysis technique (probing up to ~10 nm), and the PdNPs are largely situated within the bacterial cells, the overall proportion of Pd found by XPS (Table 2) was much lower than the Pd loading values obtained from TGA. XPS is a surface technique with a nm scale probe depth and micron scale spot size. Hence, the detection of Pd would be affected by the thickness of the thin film used for XPS analysis, the possible presence of very tiny scattered Pd nanoparticles and the uneven distribution of Pd at the spot under analysis. The reason why GO was introduced in the study was that the original biomass-supported Pd was not effective due to the Pd being inaccessible for electrocatalysis and non-conductive. This was reported for bio-Pt by Attard et al[49] This could be overcome by extensive chemical 'cleaning' (required several weeks in a series of solutions) to remove the biomass component which gave excellent electrochemistry, albeit it also resulted in nanoparticle aggregation in completely cleaned samples. The incorporation of graphene is a simple way to potentially achieve the same outcome in a single step synthesis avoiding prolonged use of aggressive chemicals. The overall proportions of carbon and oxygen, however, confirm that oxygen has been removed in varying degrees from every sample during this reduction process. The assigned components for C1s, O1s, and Pd 3d for all the samples with bacteria are shown in Table S2. The deconvoluted high resolution C 1s spectra of the various samples are shown in Figure 3.

Figure 3(a) and 3(b) show the deconvoluted C 1s spectra for B-rGO(H) and B-rGO(F) which show only partial reduction of oxygen when compared with the spectra from GO alone and *E. coli* alone (Figure S3). This applies also to the samples B-Pd(H) and B-Pd(F) which did not have any GO, confirming that the carbon in the biomass is also altered by this process, as suggested earlier by the TGA studies. However, an inspection of the C1s spectra for GO and *E. coli* (Figure S4 a and d) revealed the similarities between them. These suggested that a large proportion of the components and features visible in samples containing both GO and *E. coli* are contributed by the carbon bonds present in the biomass. Thus, the assignment of the carbon peak components in such samples i.e. B-rGO(F), B-rGO(H), B-rGO/Pd(F) and B-rGO/Pd(H), is not straightforward. While the carbon-oxygen

bonds in the biomass are also affected by this reduction process; the presence of nitrogen-containing groups in the biomass such as amine (C-N(CH_2-NH_2), occurring around 285.8 eV) and amide (N(O)-C=O occurring around 287.9 eV) overlap with the epoxide (C-OH) and carbonyl (C=O) peaks, respectively. Therefore, the presence of significantly strong components at these binding energies in samples containing GO and biomass, even after the reduction, is justified and is not suggesting incomplete reduction of carbon. The previous evidence from XRD shows that the GO is largely reduced to rGO, which supports this hypothesis. This is particularly true for samples B-rGO/Pd(H) and B-rGO/Pd(F) which, according to XRD and TGA studies, show almost complete reduction. However, the presence of closely positioned oxygen and nitrogen functional groups highlights the limitation of XPS data in identifying the true level of oxygen reduction in these samples. The above also explains why, in all samples containing bacteria, the hydroxyl groups show a relative decrease while epoxide groups show a relative increase after the reduction process (Figure 3, Table S1). It was also observed that the carbon reduction was stronger in the samples containing GO which were reduced with hydrogen when compared to those reduced with formate. Moreover, in the hydrogen-reduced samples there was a higher proportion of C=O. The mechanism of reduction appears to be favouring formation of C=O groups which are more stable. Comparing the peaks in the spectra in Figure 3 it can be seen that, in the presence of Pd, more hydroxyl and carbonyl groups are removed. This supports the evidence from XRD that the Pd improves the reduction of the GO, which is in agreement with the literature reports on Pt/rGO,[28] suggesting that metal nanoparticle nucleation on oxygen defect sites accelerates oxygen reduction in GO.

C1s spectra for various other control samples (Figure S5) further confirmed that without each element present in the system, reduction of carbon-oxygen bonds does not happen as extensively as it does in the combined presence of bacteria and a mild reducing agent. There are large peaks due to epoxide bonds remaining in all samples containing GO reduced in the presence of either *E. coli* or H_2/formate alone. It is also evident that the reduction of Pd alone using *E. coli* results in a relatively higher quantity of epoxide/amine residues though there are fewer hydroxyl groups. The exception to this low rate of reduction is the reduction of GO and Pd using H_2 (Figure S5d). However, exposure of GO and

Pd to formate alone does not result in any significant reduction of GO. Taking this evidence together with the XRD data, suggests that both the GO and Pd (II) are reduced with hydrogen alone (in the absence of any *E. coli*), but the GO appears to form amorphous carbon rather than more crystalline graphene sheets.

Palladium XPS spectra (Figure 4) were fitted using three symmetric Gaussian-Lorentzian peaks according to the method described by Chen et al.[38]. The doublet peak components in the $3d_{5/2}$ and $3d_{3/2}$ regions are constrained to have a separation of 5.26 eV and an area ratio of 3/2 (Thermo Fisher Scientific 2013). The components in the Pd $3d_{5/2}$ peak were assigned as listed in Table S2 and were in agreement with the literature[38]. The spectra in Figure 4a-d show the extent of the reduction of Pd (II) to Pd(0) in the samples. Based on the component percentage composition as obtained from the deconvolution data, on an average, between 80-85% of the Pd (II) in surface layers was reduced to Pd(0), supporting the findings of XRD and TEM. B-Pd(H) samples show relatively less Pd (0) compared to those with formate (Table S1) which could also be due to the fact that most Pd (0) formed in H_2 samples was inside the bacteria which would have relatively weaker intensity. The Pd spectra for control samples (Figure S6), revealed that using H_2 alone (Figure S6 d, j) resulted in good reduction, but reduction with formate alone resulted in large quantities of Pd (II) and bulk Pd (Figure S6 k). Tests using *E. coli* alone did not lead to any reduction, resulting in strong, intense peaks due to Pd (II) (see Figure S6d-e).

To provide further insight, Raman spectroscopy was used to analyse the carbon structure in the materials. The two main peaks of interest are the D (disorder) and G (graphitic) carbon peaks at approximately 1345 cm^{-1} and 1582 cm^{-1}, respectively[39]. Other interesting features are the 2D and D+G peaks at around 2700 and 2950 cm^{-1}, respectively. The ratio of these (I_{2D}/I_{D+G}) indicates the extent of the aromatic carbon structure versus lattice disorder. The shape and position of the 2D peak indicates the layering of the graphite planes[40]. The Raman spectra in Figure 4(e) show that in GO the G peak is found at a higher wavenumber position, and the amorphous nature of a sample shifts the D peak to lower wavenumbers, which is in agreement with the literature[39]. The I_D/I_G ratio for the reduced sample containing GO showed an increase when compared with pristine GO, suggesting an increase in

disorder for all samples after reduction. This supports the evidence for reduction of carbon and is in agreement with Ganguly et al.[41] who hypothesised that the removal of oxygen groups from GO creates more defects in the carbon structure due to loss of oxygen in the form of CO_2 etc. The B-rGO samples also revealed clearer 2D and D+G peaks (at around 2700 and 2950 cm^{-1}, respectively) than the B-rGO/Pd samples, indicating more disorder but fewer layers in the B-rGO. Moreover, comparing the formate and hydrogen reduced samples, it was found that hydrogen provides a sample with better separated 2D and D+G peaks compared with formate, suggesting there are fewer layers of graphene sheets in the B-rGO(H) than in B-rGO(F). The positions of the D and G peaks also provide information about the level of reduction[42]. The D peak in B-rGO and B-rGO/Pd samples, compared to the starting GO, showed a down-shift of up to 8 cm^{-1}, indicating an increase in amorphous nature, perhaps due to the bacterial biomass and loss of oxygen functional groups in the form of CO_2. The G peak with respect to the pristine GO displays an up-shift of 9-11 cm^{-1} for B-rGO suggesting an increase in disorder but shows almost no change (a negligible down-shift of 1-3 cm^{-1}) for B-rGO/Pd, suggesting that there is more amorphous carbon in B-rGO than in the B-rGO/Pd samples. Overall, this evidence supports the reduction of GO, and hydrogen appears to be the more effective reducing agent. The evidence here obtained from XRD and XPS supports that reduction of GO in the presence of Pd is more effective than GO alone. However, confirmed reduction of carbon in B-rGO/Pd samples based on XRD and TGA data in conjunction with no change in the G peak position for these samples compared to pristine GO samples suggested that the reduction process did not increase or induce any further disorder in the samples despite the possible loss of CO_2. The samples of Pd reduced without GO (i.e. B-Pd(F) and B-Pd(H), Figure 4f) also revealed D and G components. *E. coli* alone has no peak in this region (Figure 4e) which is consistent with previous reports[43,44]. This provides clear evidence that the carbon in the biomass was altered by the reduction processing and/or the presence of Pd (II) and further strengthens our hypothesis based on XRD and XPS analysis. The comparison of the various Raman spectra further confirmed that the GO-Pd system is more effectively reduced in the presence of both (bacteria and electron donor) elements together, than by separate reduction.

Understanding the interaction between *E. coli*, Pd (II) and GO. Based on the various material characterisation studies discussed above it is evident that the simultaneous presence of *E. coli*, mild reducing agent, GO and Pd (II) salt most certainly creates an interactive and synergistic environment allowing better control of PdNP size and their distribution on the inside of the bacterial membrane and rGO sheets. These are collective interactions and are not just limited to 'one on one' *E. coli*-GO electron exchange or Pd (II)-GO exchanges, which is why the simultaneous presence of all 4 components produces the best results. More importantly, the presence of Pd (II) and the mild reducing agents appears to encourage electronic interaction of the same with the bacterial carbon allowing simultaneous oxygen reduction in bacterial biomass and Pd nanoparticle nucleation similar to that suggested in metal-rGO systems. Consequently, there is an improved carbon structure as is clear from the Raman spectra. Based on these observations we hypothesise the following: when the bacterial cells and GO sheets exist in dispersion (Figure 1a), there is some affinity between the inner and outer membrane cytochromes and oxygen functional groups present in bacteria and GO, respectively (Figure 5), as previously suggested[34]. The addition of Pd (II) salt leads to a competitive uptake of the salt by the cells and the sheets leading to nucleation of Pd(0) on various hydrogenase and oxygen defect sites in the bacteria and GO, respectively. The addition of a mild reducing agent like hydrogen or formate as an electron donor at this stage causes the hydrogenases to release electrons[11], which are channelled by the cells to the GO sheets and the Pd (II) on the GO surface, as well as to Pd (II) nucleations on the membrane and within the bacterial cells. Consequently, the cells and rGO sheets are both decorated with Pd nanoparticles, while GO and carbon in the biomass undergo loss of oxygen species with the resultant biomass much more structured and crystalline and comparable to the reduced graphene oxide.

CONCLUSIONS

Simultaneous reduction of GO and Pd (II) was carried out in the presence of *E. coli* and H_2 or sodium formate as a mild chemical reducing agent to successfully produce a material consisting of reduced

GO-biomass composite with Pd nanoparticles decorated on the rGO sheets and bacterial cell scaffold. Detailed characterisation studies using XPS, Raman spectroscopy, XRD and TEM confirmed that: a) both the bacterial cells and the reducing agent are required for an effective reduction process, b) the presence of GO improves the reduction of Pd and vice versa and c) the Pd (II) reduction also enables simultaneous reduction of the oxygen content in the bacterial biomass. Various parameters including the presence and absence of GO and the choice of mild reducing agent (or e^- donor) were found to affect the distribution, size as well as the oxidation state (0, +2 or +4) of the PdNPs formed in these reactions. While the PdNPs formed on rGO sheets are relatively smaller (2-5 nm) compared to those formed in the bacterial scaffold; the simultaneous reduction process showed better size control and smaller particle size formation in the bacterial scaffold than those prepared in the absence of GO. Moreover, the size and distribution of the PdNPs produced also depended on the reducing agent used. Reduction using formate resulted in smaller PdNPs, which were located throughout the cells while those produced using hydrogen were largely agglomerated. The choice of reducing agent also seems to affect the GO reduction process as it was found that hydrogen reduction produced rGO sheets with fewer layers. The various control reactions also confirmed that, in the given conditions, the presence of *E. coli* also promoted GO reduction and the presence of H_2 or formate alone was not sufficient for an effective and compete reduction of GO which is in tandem with the previous literature reports[34]. The most interesting observation was that the simultaneous reduction process was found to modify the chemical and structural state of the carbon in the residual biomass such that the final product showed higher crystallinity and structure, which was clearly evident in the Raman spectral analysis.

The enhanced crystallinity in the carbon biomass following simultaneous GO and Pd (II) reduction, along with the better size and distribution control of PdNPs formed in rGO-biomass support, makes the final product potentially suitable for testing in catalyst-support studies in applications like fuel cells and electrolysis. This bacterially-driven process also has the potential to pave the way towards a more healthy precious metal economy, allowing easy and effective recycling of precious metals for 'greener' fuel cells[45]. Hence, further studies will include relocating the surface-Pd to intracellular sites and vice versa in optimisation of the methodology, electrochemical studies of this catalyst-support

system and in-depth studies investigating the effect of reaction time, proportions of Pd (II), GO and bacterial mass and pH in optimising the electrochemical behaviour of this system for potential applications.

ACKNOWLEDGEMENTS

The authors would like to thank Dr Navneet Soin at University of Bolton for help with TGA and the National EPSRC XPS Users Service (NEXUS) at Nanolabs, Newcastle University for XPS analysis. The X-ray diffractometer and the Raman microscope used in this research were accessed, through Birmingham Science City: Creating and Characterising the Next Generation of Advanced Materials (West Midlands Centre for Advanced Materials Project 1) and Birmingham Science City: Innovative Uses for Advanced Materials in the Modern World (West Midlands Centre for Advanced Materials Project 2) respectively, with support from Advantage West Midlands (AWM) and part funded by the European Regional Development Fund (ERDF). The support of EPSRC (studentship to Rachel E.Priestley via the Doctoral Training Centre '*Hydrogen, Fuel Cells and their Applications*') and grant No EP/H029567/1 is gratefully acknowledged.

REFERENCES

1. Van Meel, K.; Smekens, A.; Behets, M.; Kazandjian, P.; Van Grieken, R. Determination Of Platinum, Palladium, And Rhodium In Automotive Catalysts Using High-Energy Secondary Target X-Ray Fluorescence Spectrometry. Anal Chem 2007, 79, 6383–6389
2. Damin, I. C.; Vale, M. G. R.; Silva, M. M.; Welz, B.; Lepri, F. G.; dos Santos, W. N.; Ferreira, S. L. Palladium as chemical modifier for the stabilization of volatile nickel and vanadium compounds in crude oil using graphite furnace atomic absorption spectrometry. J Anal At Spectrom 2005, 20, 1332-1336.

3. Furst, M.R.L.; Goff, R. L.; Quinzler, D.; Mecking, S.; Botting, C. H.; Cole-Hamilton, D.J. Polymer precursors from catalytic reactions of natural oils. Green Chem 2012,14, 472-477
4. Alvarez, G. F.; Mamlouk, M.; Senthil Kumar S. M.; Scott K. Preparation And Characterisation Of Carbon-Supported Palladium Nanoparticles For Oxygen Reduction In Low Temperature PEM Fuel Cells. J Appl Electrochem 2011, 41, 952-937.
5. Antolini, E. Palladium In Fuel Cell Catalysis. Energy Environ Sci 2009, 2, 915-931
6. Zhou, Z. M.; Shao, Z. G.; Qin, X. P.; Chen, X. G.; Wei, Z. D.; Yi, B. L. Durability Study Of Pt–Pd/C As PEMFC Cathode Catalyst. Intl J Hydrogen Energy 2010, 35, 1719-1726.
7. Bonifacio, R. N.; Neto, A. O.; Linardi, M. High Performance Carbon Supported Palladium Catalyst in Anodes of Proton Exchange Membrane Fuel Cell. Int J Electrochem Sci 2013, 8, 159-167.
8. Murray, A. J.; Mikheenko, I. P.; Goralska, E.; Rowson, N. A.; Macaskie, L. E. Biorecovery of Platinum Group Metals from Secondary Sources. Adv Mater Res 2007, 651-654
9. Lloyd, J. R.; Yong, P.; Macaskie, L. E. Enzymatic Recovery Of Elemental Palladium By Using Sulfate-Reducing Bacteria, Appl Environ Microbiol 1998, 64, 4607-4609.
10. Bunge, M.; Sobjerg, L. S.; Rotaru, A. E.; Gauthier, D.; Lindhardt, A. T.; Hause, G.; Finster, K.; Kingshott, P.; Skrydstrup, T.; Meyer, R. L. Formation Of Palladium(0) Nanoparticles At Microbial Surfaces, Biotechnology and Bioengineering 2010, 107, 206-215.
11. Deplanche, K.; Caldelari, I.; Mikheenko, I. P.; Sargent, F.; Macaskie, L. E. Involvement Of Hydrogenases In The Formation Of Highly Catalytic Pd(0) Nanoparticles By Bioreduction Of Pd (II) Using *Escherichia coli* Mutant Strains. Microbiology 2010, 156, 2630-2640.
12. Ogi, T.; Honda, R.; Tamaoki, K.; Saitoh, N.; Konishi, Y. Direct Room-Temperature Synthesis Of A Highly Dispersed Pd Nanoparticle Catalyst And Its Electrical Properties In A Fuel Cell. Powder Technology 2011, 205, 143-148.
13. Yong, P.; Paterson-Beedle, M.; Mikheenko, I. P.; Macaskie, L. E. From Bio-Mineralisation To Fuel Cells: Biomanufacture Of Pt And Pd Nanocrystals For Fuel Cell Electrode Catalyst. Biotechnol Lett 2007, 29, 539-544.

14. Sobjerg, L. S.; Lindhardt, A. T.; Skrydstrup, T.; Finster, K.; Meyer, R. L. Size Control And Catalytic Activity Of Bio-Supported Palladium Nanoparticles. Colloids and Surfaces B-Biointerfaces 2011, 85, 373-378.
15. Antolini, E. Palladium In Fuel Cell Catalysis. Energy Environ Sci 2009, 2, 915-931.
16. De Carvalho, R. P.; Yong, P.; Mikheenko, I. P.; Paterson-Beedle, M.; Macaskie, L. E. Electron Paramagnetic Resonance Analysis Of Active Bio-Pd-Based Electrodes For Fuel Cells. Adv Mater Res 2009, 71-73, 737-740.
17. Salas, E. C.; Sun, Z.; Luttge, A.; Tour, J. M. Reduction Of Graphene Oxide Via Bacterial Respiration. ACS Nano 2010, 4, 4852-4856.
18. Wang, G.; Qian, F.; Saltikov, C. W.; Jiao, Y.; Li, Y. Microbial Reduction Of Graphene Oxide By *Shewanella*. Nano Research 2011, 4, 563-570.
19. Akhavan, O.; Ghaderi, E.; Toxicity Of Graphene And Graphene Oxide Nanowalls Against Bacteria. ACS Nano 2010, 4, 5731-5736.
20. Akhavan, O.; Ghaderi, E. *Escherichia coli* Bacteria Reduce Graphene Oxide To Bactericidal Graphene In A Self-Limiting Manner. Carbon 2012, 50, 1853-1860.
21. Gurunathan, S.; Han, J. W.; Eppakayala, V.; Kim, J.H. Microbial Reduction Of Graphene Oxide By *Escherichia coli*: A Green Chemistry Approach. Colloids and Surfaces B-Biointerfaces 2013, 102, 772-777.
22. Zhang, J.; Yang, H.; Shen, G.; Cheng, P.; Zhang, J.; Guo, S. Reduction Of Graphene Oxide Vial-Ascorbic Acid. Chem Commun 2010, 46, 1112-1114.
23. Park, S.; Ruoff, R. S. Chemical methods for the production of graphenes. Nature Nanotechnology 2009, 4, 217 – 224.
24. Williams, G.; Seger, B.; Kamat, P. V. TiO2-Graphene Nanocomposites. UV- Assisted Photocatalytic Reduction of Graphene Oxide. ACS Nano 2008, 2, 1487– 1491.
25. Zhu, C.; Guo, S.; Fang, Y.; Dong, S. Reducing Sugar: New Functional Molecules for the Green Synthesis of Graphene Nanosheets. ACS Nano 2010, 4 (4), pp 2429–2437

26. Liu, J.; Fu, S.; Yuan, B.; Yulin Li, Y.; Deng, Z. Toward a Universal "Adhesive Nanosheet" for the Assembly of Multiple Nanoparticles Based on a Protein-Induced Reduction/Decoration of Graphene Oxide. J Am Chem Soc 2010, 132, 7279–7281.
27. Tang, X. Z.; Cao, Z.; Zhang, H. B.; Liua, J.; Yu, Z. Z. Growth of silver nanocrystals on graphene by simultaneous reduction of graphene oxide and silver ions with a rapid and efficient one-step approach. Chem Commun 2011, 47, 3084-3086
28. Sharma, S.; Ganguly, A.; Papakonstantinou, P.; Miao, X.; Li, M.; Hutchison, J. L.; Delichatsios, M.; Ukleja S. Rapid Microwave Synthesis Of CO Tolerant Reduced Graphene Oxide-Supported Platinum Electrocatalysts For Oxidation Of Methanol. J Phys Chem C 2010, 114, 19459-19466.
29. Li, Y.; Gao, W.; Ci, L.; Wang, C.; Ajayan, P. M. Catalytic Performance Of Pt Nanoparticles On Reduced Graphene Oxide For Methanol Electro-Oxidation. Carbon 2010, 48, 1124-1130.
30. Hassan, H. M. A.; Abdelsayed, V.; Khder, A. E. R. S.; Abouzeid, K. M.; Terner, J.; El-Shall, M. S.; Al-Resayes, S. I.; El-Azhary, A. A. Microwave Synthesis Of Graphene Sheets Supporting Metal Nanocrystals In Aqueous And Organic Media. J Mater Chem 2009, 19, 3832-3837.
31. Scheuermann, G. M.; Rumi, L.; Steurer, P.; Bannwarth, W.; Mülhaupt, R. Palladium Nanoparticles On Graphite Oxide And Its Functionalized Graphene Derivatives As Highly Active Catalysts For The Suzuki−Miyaura Coupling Reaction. J Am Chem Soc 2009, 131, 8262-8270.
32. Yuan, Y.; Zhou, S.; Zhao, B.; Zhuang, L.; Wang, Y. Microbially-Reduced Graphene Scaffolds To Facilitate Extracellular Electron Transfer In Microbial Fuel Cells. Bioresource Technology 2012, 116, 453-458.
33. Bennett, J. A.; Mikheenko, I. P.; Deplanche, K.; Shannon, I. J.; Wood, J.; Macaskie, L. E. Nanoparticles Of Palladium Supported On Bacterial Biomass: New Re-Usable Heterogeneous Catalyst With Comparable Activity To Homogeneous Colloidal Pd In The Heck Reaction. Applied Catalysis B-Environmental 2013, 140, 700-707.
34. Jiao, Y. Q.; Qian, F.; Li, Y.; Wang, G. M.; Saltikov, C. W.; Gralnick, J. A. Deciphering The Electron Transport Pathway For Graphene Oxide Reduction By *Shewanella oneidensis* Mr-1. J Bacteriol 2011, 193, 3662-3665.

35. Zhong, L.-S.; Hu, J. S.; Cui, Z. M.; Wan, L. J.; Song, W. G. In-Situ Loading Of Noble Metal Nanoparticles On Hydroxyl-Group-Rich Titania Precursor And Their Catalytic Applications. Chem Mater 2007, 19, 4557-4562.
36. Fraundorf, P.; Qin, W.; Moeck, P.; Mandell, E. Making Sense Of Nanocrystal Lattice Fringes. J Appl Phys 2005, 98, 114308-
37. Wilson, N. R.; Pandey, P. A.; Beanland, R.; Young, R. J.; Kinloch, I. A.; Gong, L.; Liu, Z.; Suenaga, K.; Rourke, J. P.; York, S. J. et al.. Graphene Oxide: Structural Analysis And Application As A Highly Transparent Support For Electron Microscopy. ACS Nano 2009, 3, 2547-2556.
38. Chen, L.; Yelon, A.; Sacher, E. X-Ray Photoelectron Spectroscopic Studies Of Pd Nanoparticles Deposited Onto Highly Oriented Pyrolytic Graphite: Interfacial Interaction, Spectral Asymmetry, And Size Determination. J Phys Chem C 2011, 115, 7896-7905.
39. Ferrari, A. C. Raman Spectroscopy Of Graphene And Graphite: Disorder, Electron-Phonon Coupling, Doping And Nonadiabatic Effects. Solid State Communications 2007, 143, 47-57.
40. Childres, I.; Jauregui, L. A.; Park, W.; Cao, H.; Chen, Y. P. Raman Spectroscopy Of Graphene And Related Materials. Developments in Photon and Material Science Research, 2013
41. Ganguly, A.; Sharma, S.; Papakonstantinou, P.; Hamilton, J. Probing The Thermal Deoxygenation Of Graphene Oxide Using High-Resolution In Situ X-Ray-Based Spectroscopies. J Phys Chem C 2011 115, 17009-17019.
42. Ferrari, A. C.; Robertson, J. Interpretation Of Raman Spectra Of Disordered And Amorphous Carbon. Phys Rev B 2000, 61, 14095-14107.
43. Chan, J. W.; Winhold, H.; Corzett, M. H.; Ulloa, J. M.; Cosman, M.; Balhorn, R.; & Huser, T. Monitoring dynamic protein expression in living *E. coli*. Bacterial cells by laser tweezers Raman spectroscopy. Cytometry Part A 2007, 71, 468-474.
44. Jarvis, R. M.; Goodacre, R. Discrimination Of Bacteria Using Surface-Enhanced Raman Spectroscopy. Anal Chem 2004, 76, 40-47.

45. Yong P.; Liu W., Zhang Z.; Beauregard D, Johns M.L.; Macaskie L.E. One step bioconversion of waste precious metals into *Serratia* biofilm-immobilized catalyst for Cr(VI) reduction. Biotechnol Letts 2015, DOI 10.1007/s10529-015-1894-1.

46. Jamur M. C.; Oliver C.; Permeabilization of Cell Membranes. Methods Mol Biol 2010, 588, 63-66.

47. Panesar P. S.; Panesar R; Singh R. S.; Bera M. B. Permeabilization of yeast cells with organic solvents for β-galactosidase activity. Res J Microbiol 2007, 2, 34-41.

48. Mikheenko, I. P.; Rousset, M.; Dementin S.; Macaskie L. E., Bioaccumulation of Palladium by *Desulfovibrio fructosivorans* Wild-Type and Hydrogenase-Deficient Strains. Appl Environ Microbiol 2008, 74, 6144-6146

49. Attard G. A; Casadesús, M; Macaskie, L.E.; Deplanche K. Biosynthesis of Platinum Nanoparticles by Escherichia coli MC4100: Can Such Nanoparticles Exhibit Intrinsic Surface Enantioselectivity? Langmuir 2012, 28, 5267-5274.

FIGURE CAPTIONS

Figure 1 (a-c): TEM images of B-rGO/Pd(F), of which *(*a) and(b) are fixed and microtome sectioned B-rGO/Pd(F) and (c) drop-dried sample giving whole cell view of B-rGO/Pd(F) with Pd nanoparticles inside and some GO sheets with much smaller PdNPs grown on them sticking to the cell near bottom right area, including expanded view of an individual PdNP; (d-f) TEM images of B-rGO/Pd(H), of which: (d,e) fixed and microtome sectioned B-rGO/Pd(H) and; (f) drop-dried sample giving whole (un-sectioned) cell view of B-rGO/Pd(H), showing a stack of 8 rGO sheets with Pd nanoparticles attached to basal and edge planes of the rGO sheets (circled).

Figure 2: (a) X-ray powder diffraction patterns for GO, B-rGO(F) and B-rGO(H); (b) B-rGO(H) and B-rGO(F); (c-d): thermogravimetric analysis for samples (c) without Pd and (d) with Pd.

Figure 3: High resolution C1s XPS spectra: deconvoluted peaks for various samples. Component peaks are labelled in Figure 3a: C-C is assigned to sp^2 carbon bonds, C-OH is hydroxyl, C-O-C epoxide, C=O carbonyl and COOH carboxyl.

Figure 4: a-d: High resolution Pd3d XPS spectra: deconvoluted peaks for samples containing Pd. e-f: Raman spectra for the various test and control samples obtained using a 514 nm laser.

Figure 5: Schematic of proposed pathway for simultaneous reduction of GO and Pd (II).

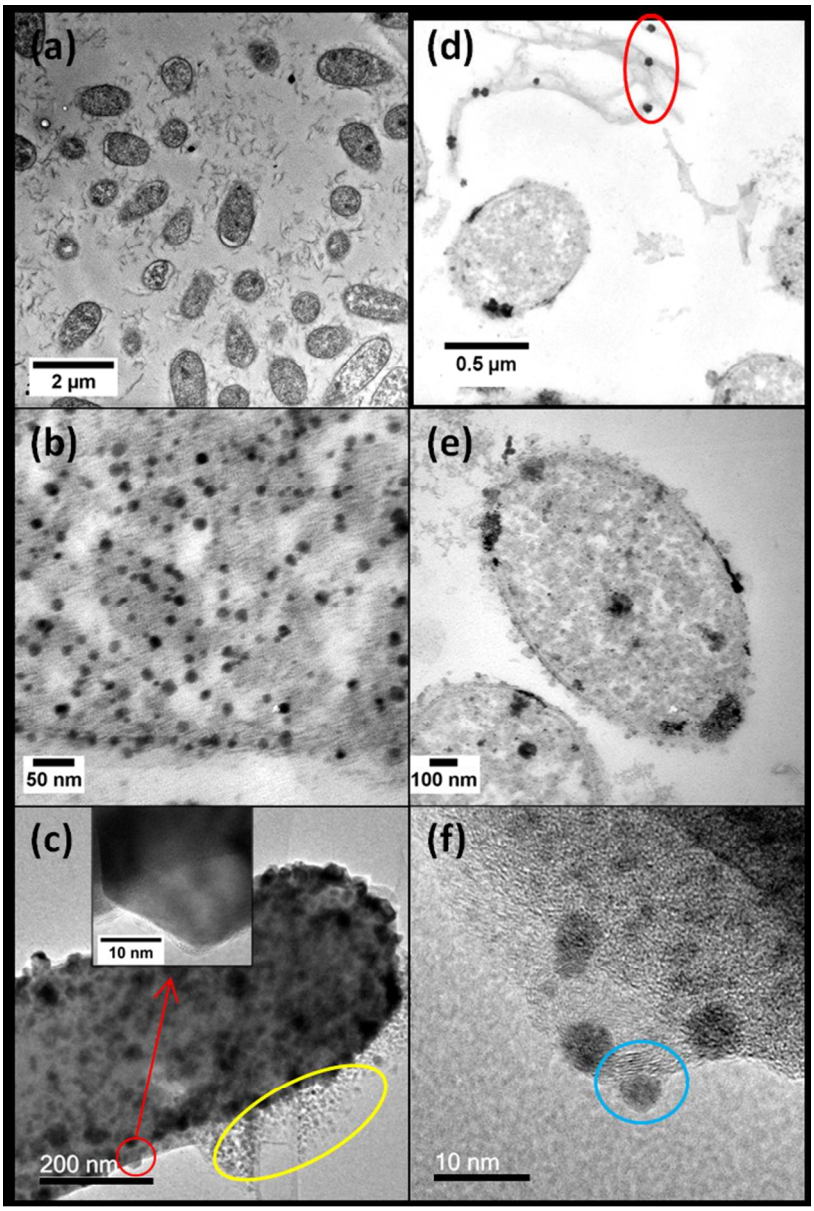

Figure 1 (a-c): TEM images of B-rGO/Pd(F), of which (a) and(b) are fixed and microtome sectioned B-rGO/Pd(F) and (c) drop-dried sample giving whole cell view of B-rGO/Pd(F) with Pd nanoparticles inside and some GO sheets with much smaller PdNPs grown on them sticking to the cell near bottom right area, including expanded view of an individual PdNP; (d-f) TEM images of B-rGO/Pd(H), of which: (d,e) fixed and microtome sectioned B-rGO/Pd(H) and; (f) drop-dried sample giving whole (un-sectioned) cell view of B-rGO/Pd(H), showing a stack of 8 rGO sheets with Pd nanoparticles attached to basal and edge planes of the rGO sheets (circled).
122x181mm (150 x 150 DPI)

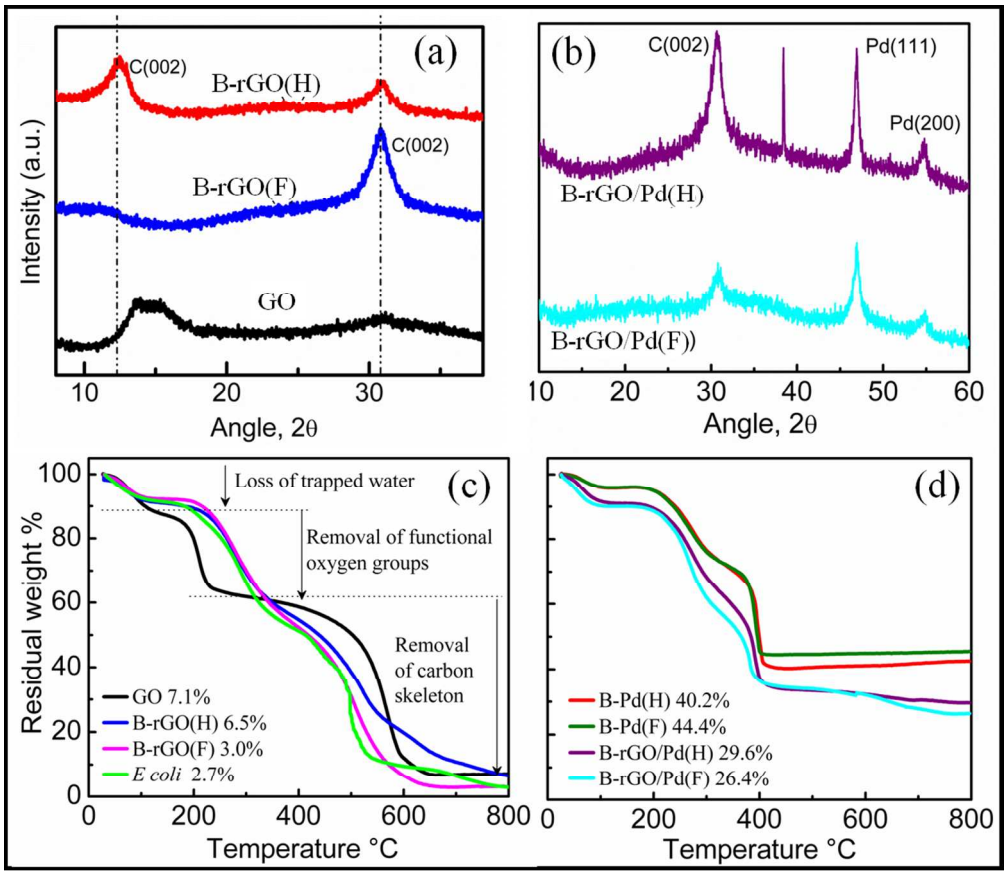

Figure 2: (a) X-ray powder diffraction patterns for GO, B-rGO(F) and B-rGO(H); (b) B-rGO(H) and B-rGO(F); (c-d): thermogravimetric analysis for samples (c) without Pd and (d) with Pd.
212x183mm (150 x 150 DPI)

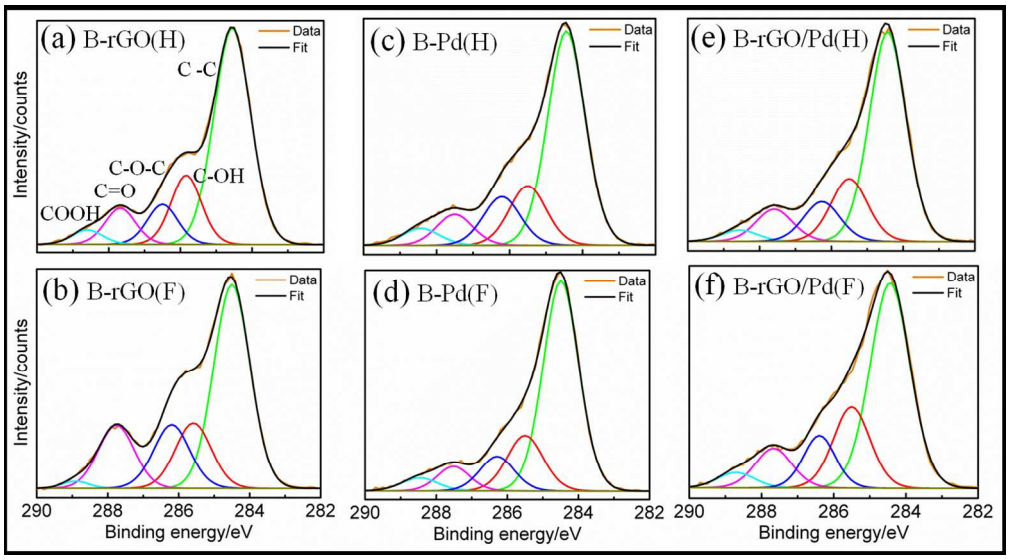

Figure 3: High resolution C1s XPS spectra: deconvoluted peaks for various samples. Component peaks are labelled in Figure 3a: C-C is assigned to sp2 carbon bonds, C-OH is hydroxyl, C-O-C epoxide, C=O carbonyl and COOH carboxyl.
261x143mm (150 x 150 DPI)

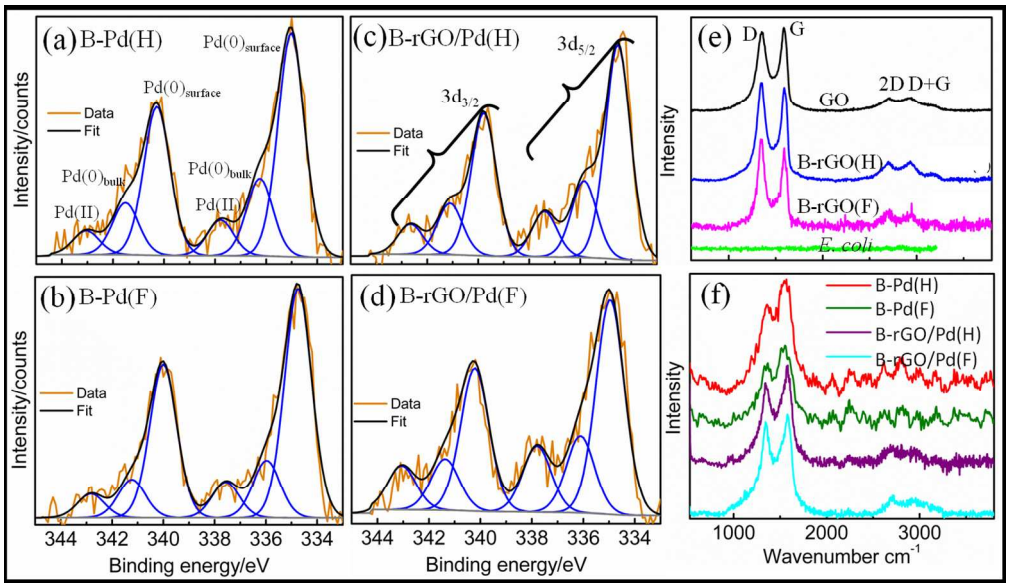

Figure 4: a-d: High resolution Pd3d XPS spectra: deconvoluted peaks for samples containing Pd. e-f: Raman spectra for the various test and control samples obtained using a 514 nm laser.
270x155mm (150 x 150 DPI)

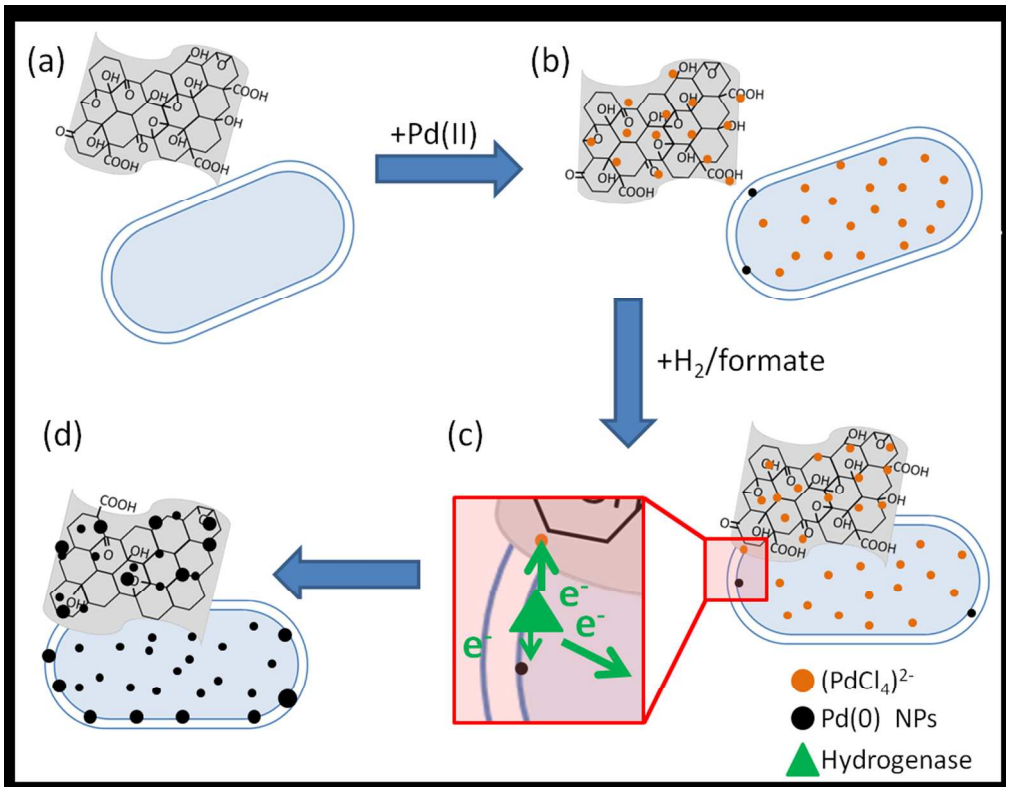

Figure 5: Schematic of proposed pathway for simultaneous reduction of GO and Pd (II).
195x152mm (150 x 150 DPI)